Eng. Sci., 2021, **16**, 288–300

Engineered Science

DOI: https://dx.doi.org/10.30919/es8d548

Spindle-like Co_3O_4-ZnO Nanocomposites Scaffold for Hydrazine Sensing and Photocatalytic Degradation of Rhodamine B Dye

Ramesh Kumar,[1] Ahmad Umar,[2, 3,*] Rajesh Kumar,[4] M. S. Chauhan,[5,*] Girish Kumar[4] and Suvarcha Chauhan[5]

Abstract

Spindle-like cobalt oxide (Co_3O_4)-zinc Oxide (ZnO) nanocomposites were synthesized by a facile low-temperature (~60 °C) solution process and well-characterized by several techniques which revealed the presence of Co_3O_4 along with ZnO in Spindle-like Co_3O_4-ZnO nanocomposites. The as-synthesized Spindle-like Co_3O_4-ZnO nanocomposites were analyzed for their photocatalytic and sensing properties. The photocatalytic degradation of the aqueous solution of Rhodamine B (RhB) was evaluated in the presence of Ultraviolet (UV) radiations. About 98% degradation of RhB was observed within just 50 min. The synthesized Co_3O_4-ZnO nanocomposites displayed prevalent photocatalytic behavior towards the photocatalytic dissociation of RhB under optimal experimental conditions than pure ZnO particles. The sensing studies were carried out by using Co_3O_4-ZnO nanocomposites modified gold electrode for hydrazine. The modified sensor exhibited good sensitivity of 23.15 μA $\mu M^{-1}cm^{-2}$and a low-detection limit of 0.05 μM with a short response time of 2 s for hydrazine. The improved photocatalytic and sensing activities of the Co_3O_4-ZnO nanocomposites toward photodegradation of RhB and sensing of hydrazine were credited to the associated effects of improved surface area and charge separation efficiencies.

Keywords: Co_3O_4-ZnO nanocomposites; Photocatalyst; Rhodamine B; Hydrazine sensor; H_2O_2 sensor.
Received: 20 September 2021; Accepted: 10 October 2021.
Article type: Research article.

1. Introduction

The accelerated and uncontrolled urbanization, industrialization, and population growth have caused serious environmental and ecological issues. Impressive intrigue has been centered on finding the solutions for effective, easy and low-cost detoxification and removal of contaminants from wastewater which are delivered into water bodies from plastics, textile, paint, pharmaceutical, and paper industries.[1–4] In particular, the textile, chemical and pharmaceutical industries release a large amount of effluent enriched with non-biodegradable and highly hazardous organic matters, which not only disrupts ecosystems but also seriously threatens human health.[5–10] These chemicals are also carcinogenic and mutagenic. The consumption of these chemicals beyond a permissible limit leads to skin ulcers, mucous film ulcers, many skin diseases, severe damage to the respiratory and digestive systems and other countless side effects.[11–15] Thus, the designing of processes and techniques is highly desired to detect and degrade these toxic organic matters efficiently.

Recently, semiconductor metal oxides have been explored for their chemical and gas sensing properties as well as for photocatalytic degradation of harmful chemicals and dyes which otherwise are considered to be non-biodegradable.[16–18] The performance of these oxides depends mainly on the surface–volume ratio and the presence of surface defects.[19–21] These two parameters can be easily tuned either by doping the metal oxides with a suitable dopant having excellent redox properties or by making composites with other semiconductor metal oxides.[22,23] One such metal oxide is ZnO, which is a n-type semiconductor with bandgap energy of ~3.4 eV.[24,25] It is widely explored for its photocatalytic,[26,27] electrochemical sensing,[28,29] fluorescence sensing,[30] gas sensing,[31,32] bio-sensing,[33,34] dye-sensitized solar cells,[35] light emitting diodes

[1]*Government College, Rajgarh District, Sirmaur-173101, Himachal Pradesh, India.*
[2] *Department of Chemistry, Faculty of Science and Arts, Najran University, Najran-11001, Kingdom of Saudi Arabia.*
[3] *Promising Centre for Sensors and Electronic Devices (PCSED), Najran University, Najran-11001, Kingdom of Saudi Arabia.*
[4] *Department of Chemistry, JC DAV College Dasuya, Hoshiarpur, Punjab, India, 144205.*
[5] *Department of Chemistry, Himachal Pradesh University, Gyan Path, Summer Hill, Shimla India, 171005.*
**Email:* ahmadumar786@gmail.com (A. Umar);
mohinderc11@gmail.com (M.S. Chauhan)

© Engineered Science Publisher LLC 2021

(LED),[36] and antimicrobial,[37–39] applications.

In contrast, Co_3O_4 is a p-type semiconductor metal oxide and is explored mainly as an active catalyst in various electro-oxidation processes,[40–42] supercapacitors,[43] anodic material for Li-ion batteries,[44] *etc*, due to its excellent redox properties attributed to $Co^{2+/3+}$redox couple.[45] Due to its p-type semiconducting nature Co_3O_4 forms hetero-interfaces with n-type semiconducting metal oxides like ZnO. In these hetero-structures, electron flow occurs from ZnO toward Co_3O_4 leading to the formation of positively charged holes (h^+) on ZnO until the attainment of the equilibrium at the hetero-junctions.[46,47] The presence of e^-– h^+ pairs at the hetero-junction improves the sensing and photocatalytic performances of the Co_3O_4/ZnO nanocomposites.[48,49]

Literature reports a variety of methods for the formation of either the doped or composite heterostructures of Co_3O_4 and ZnO. Reda *et al*.[50] followed a surfactant/template free solid-state synthetic route for the synthesis of the Co_3O_4/ZnO p-n heterostructure. This heterostructure, as photocatalyst resulted in 92.38% of photodegradation of RhB dye within 105 min of exposure to UV radiations. Co_3O_4/ZnO nanocomposites prepared via a greener microwave-assisted technique caused 80% and 90% of the degradation of MB and RhB dyes, respectively.[51] Co_3O_4@ZnO core-shell nanocomposite photo-electrodes were explored for their behavior toward photo-induced cathodic protection under visible light. The excellent photoelectrochemical properties were due to the narrow bandgap p-n junction generated at the interface of Co_3O_4 and ZnO.[52] ZnO/Co_3O_4 nanocomposite prepared via solvothermal route showed better NO_2 gas sensing performance than pure ZnO nanoparticles.[53] Co_3O_4 quantum dots/ZnO nanocages p-n nano-heterojunctions synthesized through an innovative one-off processing ZIF-8@ZIF-67 under optimum heat treatments exhibited promising trimethylamine gas sensing characteristics.[54] Similarly, Co_3O_4/ZnO nanocomposite synthesized via a one-step hydrothermal route also showed excellent triethylamine sensing performance.[49]

Though the photocatalytic activities of the Co_3O_4/ZnO nanocomposites have been exhaustively reported, however, the scope of improving the photocatalytic performance, in particular, the photodegradation time can still be significantly lowered by controlling the composition of the nanoparticles. Further reports for the electrochemical sensing of the hydrazine are rarely reported for Co_3O_4/ZnO nanoparticles. Herein, the Co_3O_4-ZnO nanocomposites were prepared through a low-temperature precipitation method followed by detailed characterization through different techniques. As-synthesized Co_3O_4-ZnO nanocomposites were explored for their photocatalytic activities towards RhB dye, generally used as water tracer dye. Further, the Au electrode modified by Co_3O_4-ZnO nanocomposites was explored for electrochemical sensing of hydrazine. Hydrazine is a highly toxic ammonia derivative used for the preparation of polymer foams, as polymerization catalysts, and for the preparation of pesticides. As photocatalyst Co_3O_4-ZnO nanocomposites showed excellent degradation efficiencies towards RhB dye. Additionally, excellent electrochemical sensing behavior was reported for hydrazine. The possible photocatalytic and sensing mechanisms of the Co_3O_4-ZnO nanocomposites were also proposed.

2. Materials and methods

2.1 Materials

Zinc nitrate hexahydrate [$Zn(NO_3)_2 \cdot 6H_2O$], Cobalt nitrate hexahydrate[$Co(NO_3)_2 \cdot 6H_2O$] and sodium hydroxide (NaOH) of AR grade were purchased from Sigma–Aldrich. Rhodamine B (RhB) was purchased from M.P. Biomedicals. All the chemicals were used as received without any further refinement. Deionized (DI) water was utilized for the preparation of analyte solutions for photocatalytic and sensing applications.

2.2 Synthesis and characterization of spindle-Like Co_3O_4-konggeZnO nanocomposites

Synthesis of Co_3O_4-ZnO nanocomposites was carried out through a simple facile procedure in which100 ml of 0.025M $Zn(NO_3)_2 \cdot 6H_2O$ was mixed with 100 ml of 0.00025M $Co(NO_3)_2 \cdot 6H_2O$ solution. After that, 100 ml of 0.025M NaOH solution was added dropwise to the reaction mixture. The mixture was subjected to vigorous stirring for 30 minutes and then finally refluxed at an optimized reaction condition of 60 °C for 6 h, followed by cooling to room temperature after the completion of the reaction. The obtained precipitates of Co_3O_4-ZnO nanocomposites were washed several times with DI water followed by ethanol and then dried at room temperature.

The morphological investigations of as-synthesized spindle-like Co_3O_4-ZnO nanocomposites were done by field emission scanning electron microscopy (FESEM) JEOL-JSM-7600F, whereas elemental analysis was conducted by using energy dispersive spectroscopy (EDS). The structural analysis of the sample was carried out by X-ray diffractometer (XRD; PANalytical X'Pert PRO) measured with Cu- Kα radiations (λ= 1.542 Å) in the range of 10–80° with a scan speed of 8°/min. To examine the optical properties of as-synthesized Co_3O_4-ZnO nanocomposites room-temperature UV–Vis spectrum (Carry 100 Bio UV–Vis spectrophotometer) was recorded. The detailed chemical analysis was done by using FTIR (Perkin Elmer-FTIRSpectrum-100) spectroscopy.

2.3 Photocatalytic degradation of rhodamine B (RhB) using spindle-like Co_3O_4-ZnO nanocomposites

To study the photocatalytic activity of as-synthesized Spindle-like Co_3O_4-ZnO nanocomposites, the photocatalytic degradation of RhB was performed using different amounts of Co_3O_4-ZnO nanocomposites under UV irradiation. The degradation of RhB was analyzed by measuring the absorbance of the aliquots at regular time intervals using UV-Visible spectrophotometer Cary 100 Bio at λ= 554 nm. The degradation reaction was performed in a 250 ml beaker, which

© Engineered Science Publisher LLC 2021

contained an aqueous solution of RhB and dispersed Co_3O_4-ZnO nanocomposites through sonication, as photocatalyst. A 125 W Mercury lamp was used as a source of the UV radiations. The rate of degradation for the decomposition of RhB was estimated by evaluating the change in absorbance. The photocatalytic percent degradation was calculated by using Eq. 1.

$$\text{Degradation} = \frac{A_o\text{-}A}{A_o} \times 100\% \quad (1)$$

where A_o=Initial absorbance of aqueous RhB solution in the absence of photocatalyst and UV exposure and A = absorbance of RhB in reaction suspensions containing the calculated amount of the photocatalyst under UV exposure for a definite time interval.

2.4 Fabrication of hydrazine chemical sensor using spindle-like Co_3O_4-ZnO nanocomposites

Au electrode was polished with 0.1 μM alumina slurry, and then ultrasonicated in a mixed solution of DI water and ethanol for 10 min. The cleaned and dried Au electrode was modified by casting the slurry of Co_3O_4-ZnO nanocomposites prepared by adding an appropriate amount of prepared nanoparticles and butyl carbitol acetate as a binder. Further, the electrode was dried at 60 ± 5 °C for 4–6 h to get a uniform layer over the entire electrode surface. The electrochemical experiments were conducted with a Metrohm Autolab B.V. Type PGSTAT 128N cyclic voltammeter using the three-electrode configuration in which the modified Au electrode, Pt wire and Ag/AgCl (sat. KCl) were used as working, counter and reference electrodes at room temperature. Phosphate buffer solution of concentration 0.1 M having pH 7.0 was used as a blank solution. This solution was used for the preparation of hydrazine analyte solution for cyclic voltammetric and amperometric studies. For amperometric analysis, a constant potential of 0.32 V was applied for different concentrations of hydrazine.

3. Results and Discussion

3.1 Structural and morphological characterization of spindle-like Co_3O_4-ZnO nanocomposites

To examine the general morphology and size of as-synthesized Co_3O_4-ZnO nanoparticles, FESEM was used (Figs.1(a)-(c)). From low magnification FESEM images (Figs.1(a, b)) we can conclude that particles are grown in high density with spherical and spindle shapes. A high magnification FESEM image (Fig. 1(c)) reveals the agglomeration of the nanoparticles. Most of the nanoparticles possessed a spindle shape with tapered ends with lengths ranging from 100–120 nm, whereas the thickness at the middle was about 100 nm. However, some other irregular shapes for Co_3O_4-ZnO nanoparticles were also observed in the FESEM images. To determine the chemical compositions and purity of Co_3O_4-ZnO nanoparticles, the EDS spectrum was recorded as shown in Fig. 1(d). There is a clear indication from the spectrum that the synthesized sample contains only Zn, O, Co, and no other impurity elements. The composition of Co_3O_4-ZnO nanocomposites was estimated to be at 67.87, 25.65, and 6.48 wt% respectively for Zn, O, and Co as shown in the inset of Fig. 1(d).

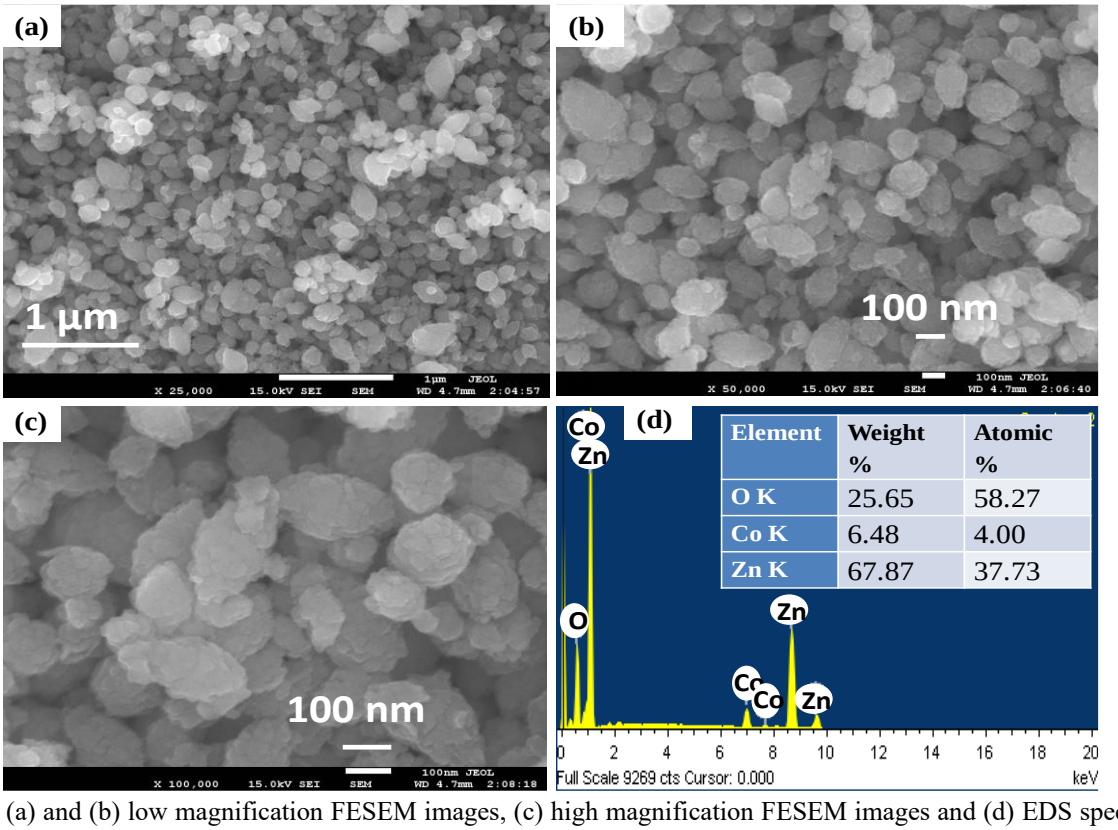

Element	Weight %	Atomic %
O K	25.65	58.27
Co K	6.48	4.00
Zn K	67.87	37.73

Fig. 1 Typical (a) and (b) low magnification FESEM images, (c) high magnification FESEM images and (d) EDS spectrum (Inset: Elemental composition) of Spindle-like Co_3O_4-ZnO nanocomposites.

© Engineered Science Publisher LLC 2021

Fig. 2(a) shows the XRD pattern of the spindle-like Co_3O_4-ZnO nanocomposites. The apparent diffraction peaks at 2θ values of 18.81°, 36.89°, 44.81°, 59.24° and 65.24° are assigned to the crystal planes (111), (311), (400), (511) and (440), respectively and are the characteristic peaks of the cubic spinel phase of Co_3O_4. The data is consistent with the JCPDS card No 42-1467 and the reported literature.[55,56] Other peaks at 2θ values 31.57°, 34.40°, 36.20°, 47.64°, 56.68°, 62.84°, 66.31°, 67.99°, 69.06 °, 72.41° and 76.91° correspond to the crystal planes of (100), (002), (101), (102), (110), (103), (200), (112), (201), (004) and (202), respectively and are the characteristic peaks of wurtzite hexagonal phase of ZnO, which can be confirmed from the reported literature.[57–59] and the JCPDS card No 36-1451. The sharpness and intensity of the observed peaks indicate the high crystallinity of synthesized Co_3O_4-ZnO nanoparticles. The crystallite size (d) of the Co_3O_4-ZnO nanoparticles was calculated using the Debye-Scherer equation (Eq. 2).[60]

$$d = \frac{0.90\,\lambda}{\beta\cos\theta} \quad (2)$$

where λ = 1.542 Å (Source wavelength), θ = Diffraction angle, β = full width half maximum (FWHM). Five high-intensity diffraction peaks were considered for the calculation of FWHM values. The corresponding crystal parameters are portrayed in Table 1. The average particle size for Co_3O_4-ZnO nanocomposites was 19.95 nm.

Table 1. Crystalline parameters for Spindle-like Co_3O_4- ZnO nanocomposites.

Diffraction planes (*hkl*)	Diffraction angles (°)	FWHM (β)	The crystallite size (nm)
ZnO (100)	31.57	0.40501	20.40
ZnO (002)	34.40	0.40038	20.79
ZnO (101)	36.20	0.50053	16.71
ZnO (102)	47.64	0.39830	21.82
ZnO (110)	56.68	0.45095	20.03

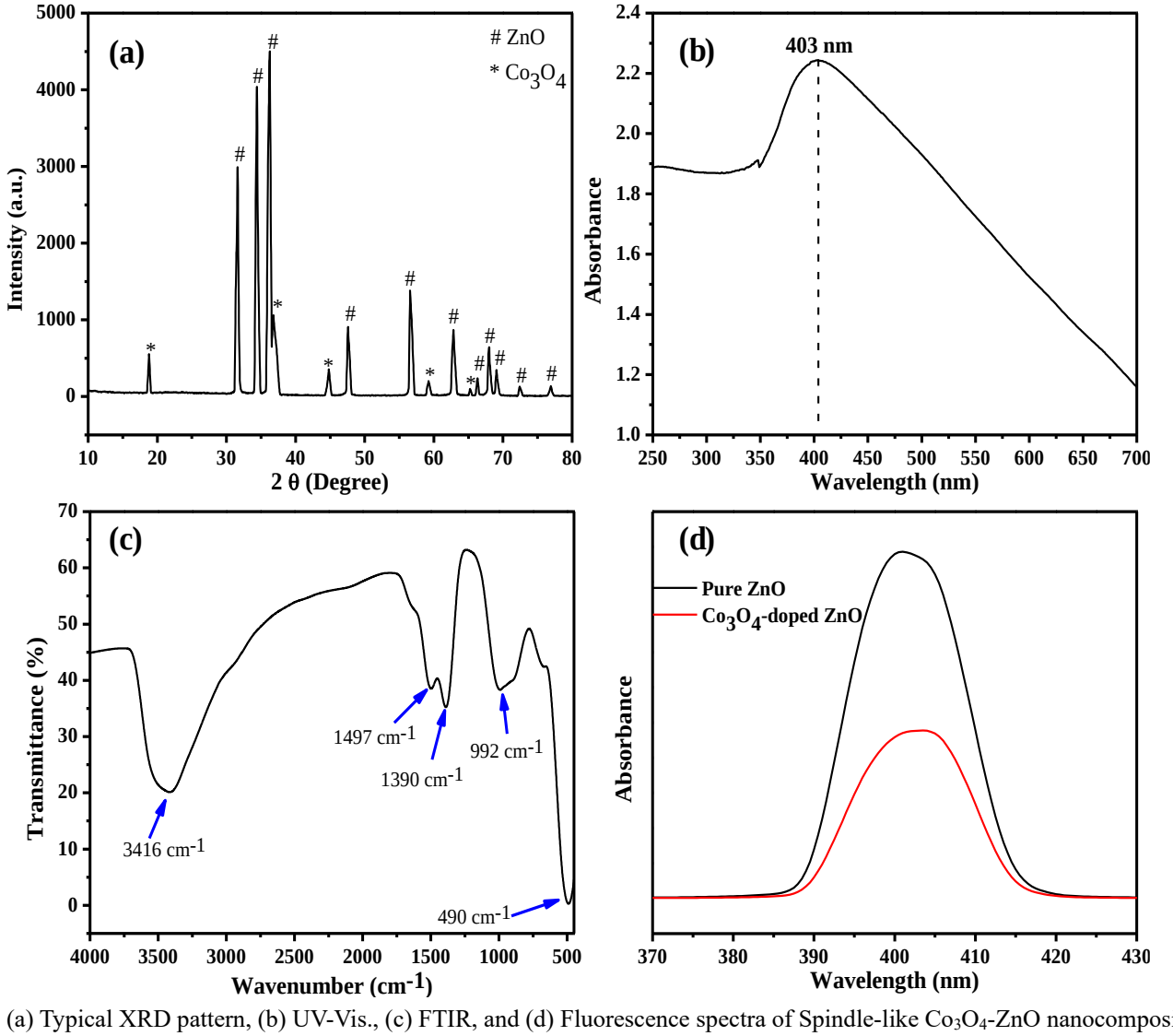

Fig. 2 (a) Typical XRD pattern, (b) UV-Vis., (c) FTIR, and (d) Fluorescence spectra of Spindle-like Co_3O_4-ZnO nanocomposites.

© Engineered Science Publisher LLC 2021

Fig. 2(b) shows the room temperature optical absorption spectra of spindle-like Co_3O_4-ZnO nanocomposites. We observe a sharp absorption peak in the UV region with a broad absorption range in the visible region, which can be attributed to the doping of Co_3O_4 in the ZnO matrix within the employed concentration range of dopant. The optical energy gap (E_g) of the Co_3O_4-ZnO nanocomposites was calculated by using Plank's equation (Eq. 3).

$$E_g = \frac{hc}{\lambda \max} = \frac{6.626 \times 10^{-34} Js \times 3 \times 10^{8} ms^{-1}}{403 \times 10^{-9} m \times 1.6 \times 10^{-19} J.eV^{-1}} = 3.08\ eV \quad (3)$$

where E_g is the bandgap energy, h is the Planks' constant (6.626×10^{-34} Js), c is the velocity of light (3×10^{8} m/s), and λ_{max} = 403 nm. The calculated optical band gap of as-synthesized Co_3O_4-ZnO nanocomposites was found to be 3.03 eV. Further, the direct band gaps of pure Co_3O_4 and ZnO are estimated to be 2.76 and 3.40 eV respectively, whereas the presence of a single peak at 403 nm corresponding to 3.08 eV bandgap in the case of spindle-like Co_3O_4-ZnO nanocomposites, indicates well mixing of the cubic phase of the Co_3O_4 and Wurtzite hexagonal phase of ZnO.

The chemical composition of Co_3O_4-ZnO nanocomposites was investigated by FTIR spectroscopy carried out at room temperature between 450–4000 cm^{-1} shown in Fig. 2(c). Several peaks at 490, 992, 1390, 1497 and 3416 cm^{-1} were found in the FTIR spectrum. The vibrational peak near 490 cm^{-1}corresponds to the M-O bond which arises from the stretching mode of the Zn-O and Co-O bonds.[24,25] The small but sharp peak at 1457 $cm^{-1}$is due to the bending vibration mode water. A well-defined absorption band at 3416 cm^{-1} is related to the O-H stretching vibrations for the physisorbed water molecules.[28,32]

To obtain information regarding defects and recombination of charge carriers present in pure ZnO and Co_3O_4-ZnO nanocomposites, we recorded the fluorescence spectra at an excitation wavelength of 390 nm of pure ZnO and Co_3O_4-ZnO nanocomposites. It is clear from Fig. 2(d) that pure and Co_3O_4-ZnO samples exhibit strong emission peaks around 400 nm corresponds to zinc vacancy-related defects. A sharp decrease in peak intensity was observed in the presence of spindle-like Co_3O_4-ZnO nanocomposites compared to pure ZnO signifies the lower recombination rate of charge carriers. We can thus conclude that doping of ZnO nanomaterials with Co_3O_4 will significantly enhance the photocatalytic and sensing efficiency.

3.2 Photocatalytic degradation of RhB dye using Co_3O_4-ZnO nanocomposites

The organic dyes released by textile industries are considered as one of the major water pollutants because of their high resistance to chemical, biological, and photochemical degradation. The degradation efficiency of spindle-like Co_3O_4-ZnO nanocomposites was studied using RhB as a model dye under UV radiations. To evaluate the photocatalytic performances, a mixture of 100 ml of 10 ppm RhB dye and different amounts of Co_3O_4-ZnO photocatalyst for various time intervals was irradiated with UV radiation. The change in absorbance value is observed as a function of UV radiation exposure time and the photocatalyst concentration to determine the percent rate of degradation.

Effect of Co_3O_4-ZnO nanocomposites dosage of photodegradation of RhB

After establishing the synthesis and characterization of spindle-like Co_3O_4-ZnO nanocomposites, the synthesized nanoparticles were studied for their photocatalytic abilities for RhB degradation as a function of UV radiations. In a typical reaction procedure, various concentrations of spindle-like Co_3O_4-ZnO nanocomposites (0.05, 0.10, and 0.15 g) were individually mixed with 100ml of RhB solution (10 ppm) then stirred for 1 hr to attain the absorption ⇌ desorption equilibrium. The reaction mixture was then exposed to a UV light source maintained at a constant distance of 20 cm from the beaker and was continuously stirred to ensure full suspension of the particles throughout the experiment. The absorption intensities of the aliquots were measured with the help of a UV-visible spectrophotometer at λ_{max} 554 nm. Fig. 3(a) represents the change in absorption intensity (A/A_o) while Fig. 3(b) gives the percentage photodegradation of RhB as a function of photocatalyst dosages. Scrutiny of the obtained results revealed that up to 98% degradation was observed within 50 minutes using 0.15g of Co_3O_4-ZnO against 10ppm RhB, however about 88 and 80% photodegradations were observed using 0.10 and 0.05g of the photocatalyst. It was observed that the spindle-like Co_3O_4-ZnO nanocomposites showed better photocatalytic performances compare to the pure ZnO nanoparticles (Fig. 3(c)). From these results, it is concluded that Co_3O_4 as a dopant efficiently improved the photocatalytic degradation of the RhB. Based upon Langmuir-Hinshelwood pseudo-first-order kinetic, Eq. 4 was used to analyze the kinetics of the photodegradation of the RhB dye by spindle-like Co_3O_4-ZnO nanocomposites.[25,37,58,61] The kinetics graph was plotted between $\ln\frac{C_o}{C}$ and radiation time exposure (t) keeping the intercept = 0.

$$\ln\frac{C_o}{C} = kt + 0 \quad (4)$$

where C_o = initial dye concentration, C = dye concentration after UV radiation exposure time (t), k = rate constant (min^{-1}).

The photodegradation of RhB followed pseudo-first-order kinetics in the presence of spindle-like Co_3O_4-ZnO nanocomposites as a photocatalyst, since a straight-line is obtained. The value of the k is equal to the slope *i.e.* 6.869×10^{-2} min^{-1} of the linear plot (Fig. 3(d)). The corresponding half lifetime $t_{1/2}$ was as low as 10.08 min. This indicates a very fast degradation of RhB dye and highly efficient photocatalytic activity of the spindle-like Co_3O_4-ZnO nanocomposites.

Fig. 4(a) is representing the molecular structure of the RhB dye whereas Fig. 4(b) is exhibiting the real-time changes of the absorption intensities as a function of UV radiation exposure time for the photodegradation of RhB in the presence

© Engineered Science Publisher LLC 2021

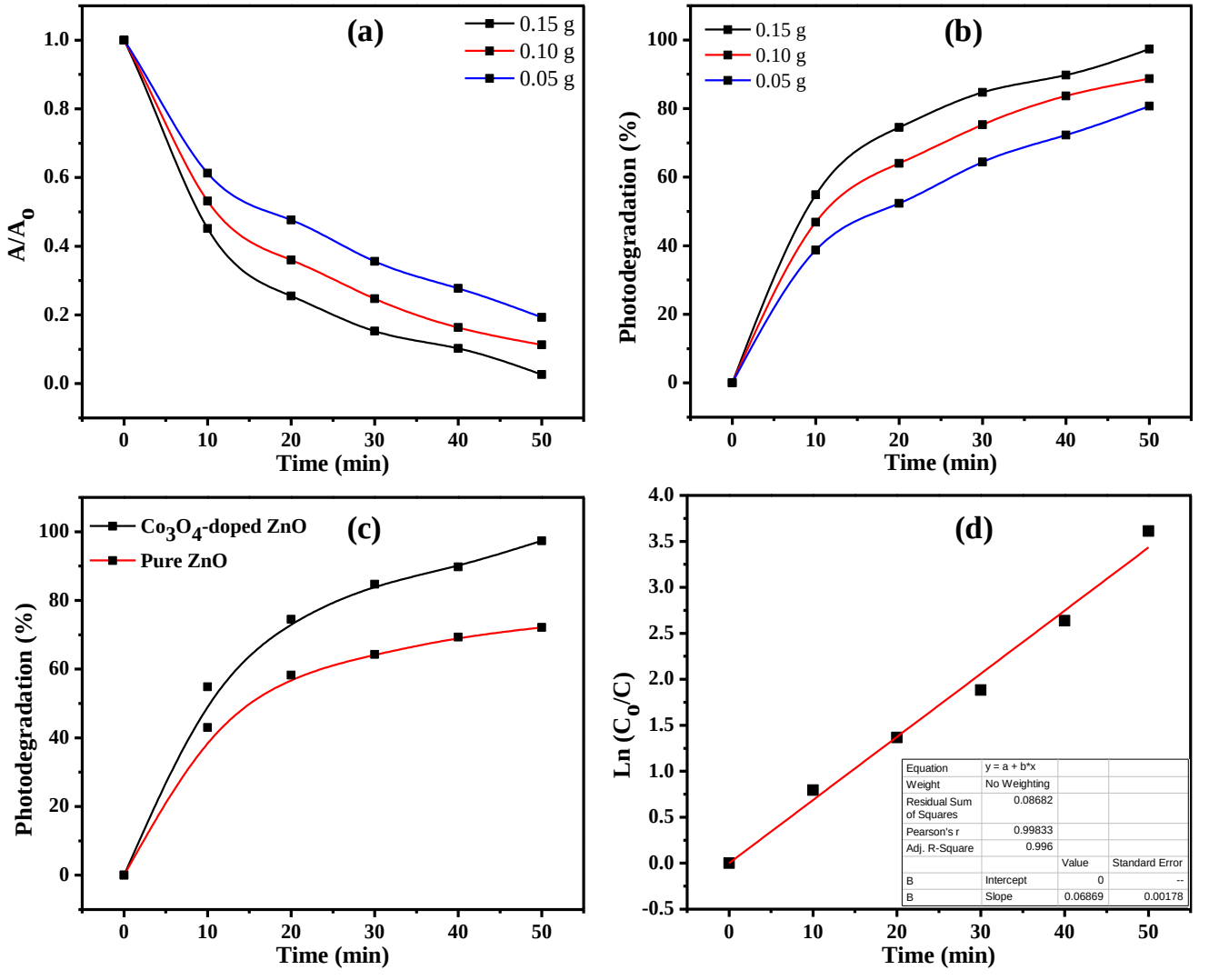

Fig. 3 (a) A/Ao variations for RhB dye, (b) Percentage photodegradation as a function of spindle-like Co_3O_4-ZnO nanocomposites dosage, (c) Comparative percent photodegradation by pure ZnO and spindle-like Co_3O_4-ZnO nanocomposites *vs.* irradiation time and(d) Pseudo-first order kinetics for RhB dye in presence of spindle-like Co_3O_4-ZnO nanocomposites as photocatalyst.

of spindle-like Co_3O_4-ZnO nanocomposites. For all the absorbance plots a strong absorption band $\lambda_{max.}$ 554 nm can be seen. The decrease in the absorption maxima with irradiation time confirms the degradation of the RhB dye and the efficient photocatalytic activity of spindle-like Co_3O_4-ZnO nanocomposites.

The state-of-art comparison of the photocatalytic efficiency of the spindle-like Co_3O_4-ZnO nanocomposites for RhB as compared to recently reported other metal oxide photocatalysts is shown in Table 2.[62-70]

The better photocatalytic activity of spindle-like Co_3O_4-ZnO nanocomposites as photocatalyst than pure ZnO is due to the synergism between Co_3O_4 and ZnO metal oxides along with better charge separation than pure ZnO. Under photo-induction, electrons from the valance band (VB) are excited to the conduction band (CB).[71] For better photocatalytic effects, there should be the presence of a sufficient number of free electrons in CB and positively charged holes (h^+) in the VB of the semiconductor metal oxide.[72,73] These species are responsible for the formation of oxygenated free radicals and anions which cause the photocatalytic degradation of the dyes. The low bandgap of Co_3O_4 (2.76 eV) results in fast e^-– h^+ recombination while a large bandgap of 3.40 for ZnO forbids the transitions of the electrons from the VB to the CB.[74] This reduces the sufficient number of h^+ in the VB and free electrons in the CB. In contrast, an intermediate bandgap of 3.08 eV for spindle-like Co_3O_4-ZnO nanocomposites is quite appropriate and avoids both these limitations. The photo-induced electrons and holes relocate at the surface of the spindle-like Co_3O_4-ZnO nanocomposites to react with the adsorbed O_2 and result in the formation of highly reactive free radicals such as $O_2^{-\bullet}$, $HO_2^{\bullet}$, and $HO^{\bullet}$ through a series of reactions (Eqs. 5-10).[75] There is a fast electron transfer from the CB of the p-type Co_3O_4 into the CB of n-type ZnO while holes are transferred from the VB of ZnO to the VB of the Co_3O_4 (Fig. 5).[76]

$$O_2 + ZnO(e^-_{CB}) \rightarrow O_2^{-\bullet} \quad (5)$$

$$O_2^{-\bullet} + H_2O \rightarrow HO_2^{\bullet} + OH^- \quad (6)$$

$$2\,HO_2^{\bullet} \rightarrow H_2O_2 + O_2 \quad (7)$$

© Engineered Science Publisher LLC 2021

Table 2. Comparative analysis of the photodegradation efficiency of spindle-like Co_3O_4-ZnO nanocomposites for RhB as compared to other reported photocatalysts.

Photocatalyst	[Dye] (ppm)	Catalyst dosage (g/100 mL)	Irradiation time (min)	Degradation (%)	Ref.
Co_3O_4/ZnO nanocomposite	10	0.01	400	89.0	[51]
CeO_2/Y_2O_3 heterostructures	20	0.04	60	98.0	[62]
TiO_2/ZrO_2 composites	10	0.05	270	90.5	[63]
ZnO nano/micro materials	2.5	0.005	180	100.0	[64]
3D flower sphere-like BiOI/Fe_3O_4 microspheres	20	0.05	30	96.5	[65]
Nanostructured Zn doped Cobalt ferrite	10	0.031	180	100.0	[66]
CdS/ZnO nanorod	5.0×10^{-5} M	0.001	480	85.0	[67]
ZnO nanostructures	10	0.1	120	97.0	[68]
ZnO nanoparticles	10	0.15	70	95.0	[69]
ZnO–Ag nanocomposite	5	0.05	30	100.0	[70]
Spindle-like Co_3O_4- ZnO nanocomposites	10	0.15	50	98.0	This work

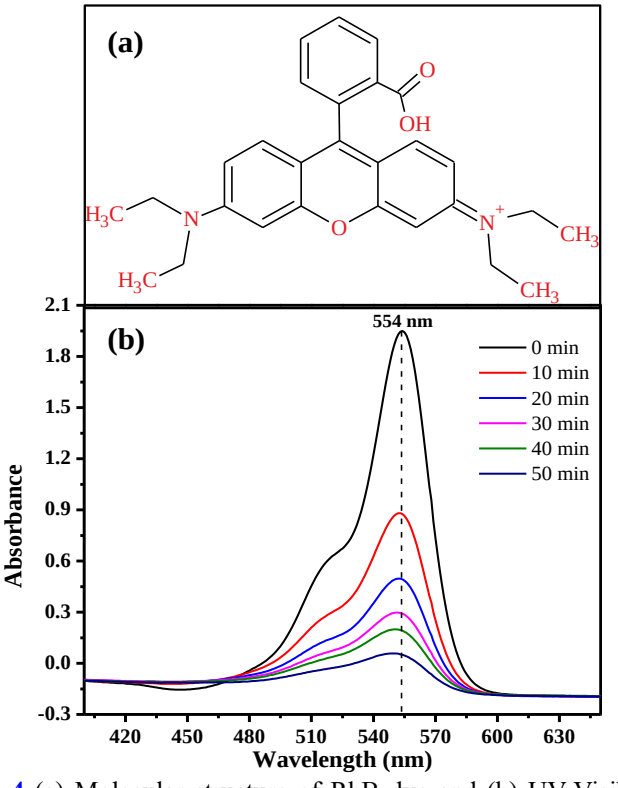

Fig. 4 (a) Molecular structure of RhB dye and (b) UV-Visible spectra of RhB (10ppm) containing 0.15g of spindle-like Co_3O_4-ZnO nanocomposites at different intervals of time.

$$H_2O_2 + O_2^{-\bullet} \rightarrow OH^{\bullet} + OH^{-} + O_2 \quad (8)$$

$$Co_3O_4(h^{+}_{VB}) + H_2O \rightarrow OH^{\bullet} + Co_3O_4 \quad (9)$$

$$OH^{\bullet} + RhB \rightarrow \text{Degradation products} \quad (10)$$

3.3 Voltammetric response of Co_3O_4-ZnO nanocomposites modified gold electrode towards oxidation of hydrazine

The electrocatalytic behavior of spindle-like Co_3O_4-ZnO nanocomposites was evaluated by carrying out a hydrazine oxidation reaction. The CV responses of the Au modified hydrazine chemical sensor are shown in Fig. 6 in the absence and presence of 1.0 mM hydrazine at the scan rate of 100 mV/s. There was no obvious redox peak observed in the case of 0.1M PBS solution (pH=7). However, a dramatic enhancement in anodic peak (Ipa=13.02 µA) was observed at the potential of 0.32 V with 1.0 mM hydrazine under the same experimental conditions. This rapid increase in current exhibits the faster electron exchange in the case of spindle-like Co_3O_4-ZnO nanocomposites modified Au electrode. Therefore, spindle-like Co_3O_4- ZnO nanocomposites can be served as a potential scaffold for electrochemical detection of hydrazine.

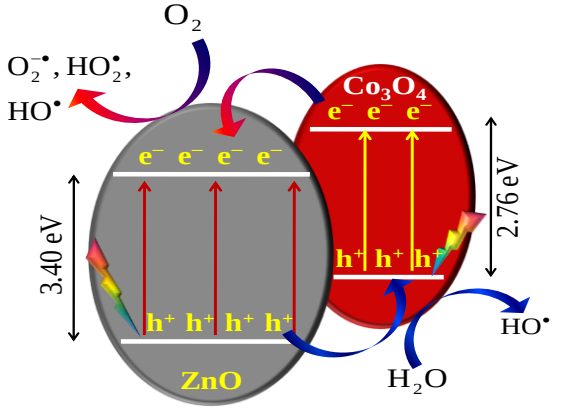

Fig. 5 The proposed photocatalytic mechanism for the RhB dye degradation by spindle-like Co_3O_4-ZnO nanocomposites.

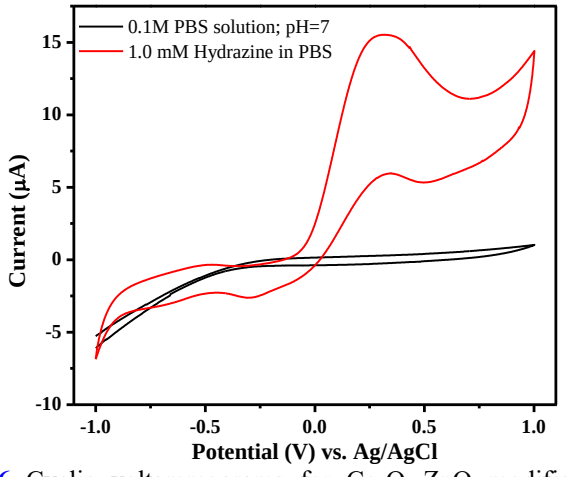

Fig. 6 Cyclic voltammograms for Co_3O_4-ZnO modified Au electrode in 0.1M PBS (pH=7) and in 1.0 mM hydrazine prepared in PBS (Scan rate = 100 mV/s).

© Engineered Science Publisher LLC 2021

3.3.1 Effect of scan rates on electro-oxidation of hydrazine

The influence of increasing scan rates, varying from 50-1000 mV/s on the anodic peak current was investigated and is illustrated in Fig. 7(a). It exhibited a linear relationship between anodic peak current *vs.* square root of the scan rate ($\nu^{1/2}$) with R^2 = 0.99184 (Fig. 7(b)). Hence electro-catalytic oxidation of hydrazine on the modified electrode is controlled by diffusion.

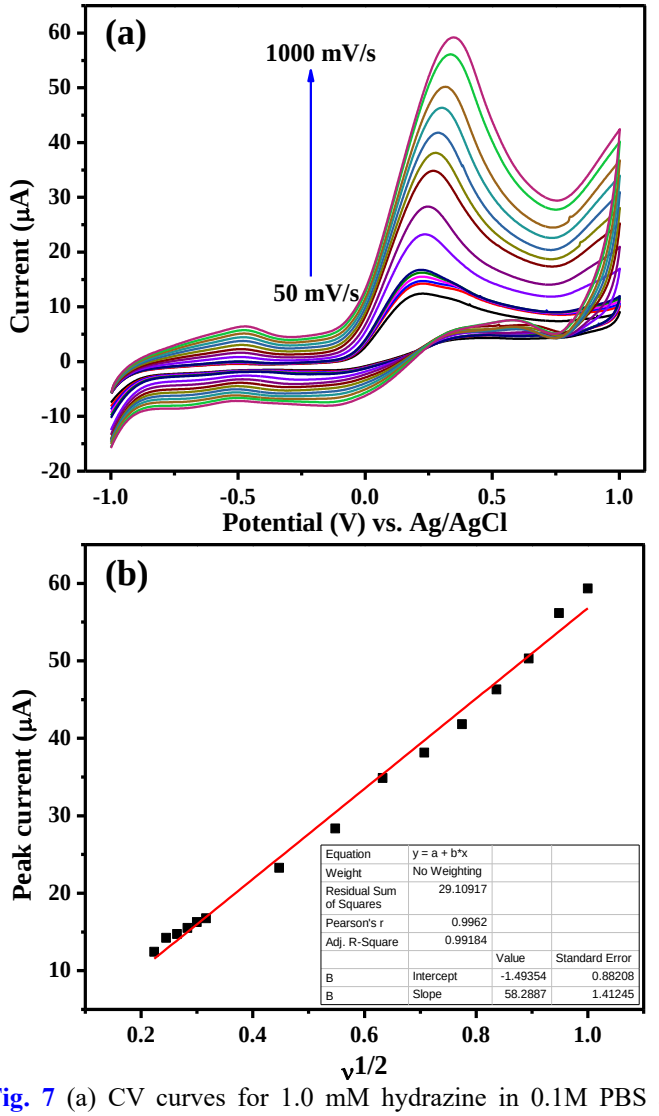

Fig. 7 (a) CV curves for 1.0 mM hydrazine in 0.1M PBS at different scan rates 50-1000 mV/s and (b) Plot for the dependence of anodic peak current with the square root of scan rate ($\nu^{1/2}$).

3.3.2 Amperometric behavior of Co_3O_4-ZnO nanocomposites modified Au electrode for hydrazine

To further investigate the performance of as-synthesized spindle-like Co_3O_4-ZnO nanocomposites towards hydrazine sensing in detail, amperometric analysis was examined under stirred conditions since amperometry under stirred conditions gives better current sensitivity as compared to voltammetry. Fig. 8(a) illustrates the current-time response of the as-fabricated electrode with the successive additions of hydrazine in 0.1M PBS (pH=7) in the time interval of 100 sec. at 0.34 V. With the addition of hydrazine, the electrocatalytic current increased abruptly and obtained a steady-state within 2s, manifesting a quick response time for the as-fabricated sensor. A corresponding calibration curve is plotted in Fig. 8(b). The sensitivity of the as-fabricated electrode was evaluated from the slope of the calibration curve. It showed a high and reproducible sensitivity value of 23.15 $\mu A \cdot \mu M^{-1} \cdot cm^{-2}$ with R^2=0.97487. The detection limit was calculated to be 0.05 μM based on the signal-to-noise ratio (S/N). Moreover, the response current is linear with increased hydrazine concentration (0.05 μM – 2.35 μM).

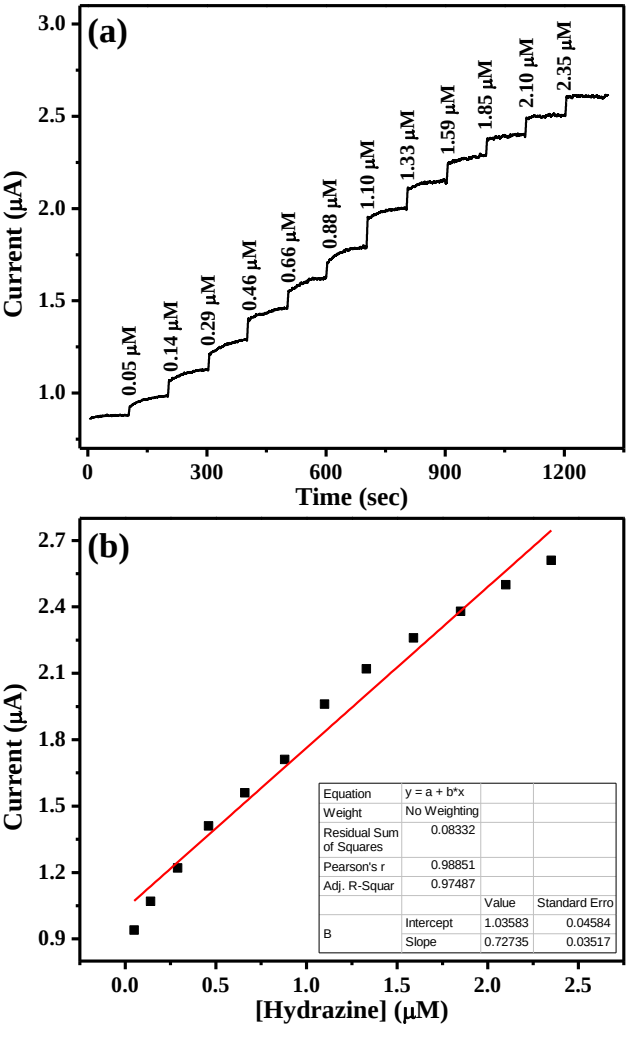

Fig. 8 (a) The amperometric response of the fabricated Au electrode with successive additions of hydrazine into 0.1 M PBS buffer solution (pH 7.0) at the time gap of 100 sec. and (b) Calibration plot between current *vs.* hydrazine concentrations.

The electrochemical hydrazine detection parameters such as sensitivity, response time, the limit of detection, and linear dynamic range are compared with earlier reported hydrazine sensors (Table 3). The data reveals that the spindle-like Co_3O_4-ZnO nanocomposites modified Au electrode is a superior electrochemical sensor as compared to other hydrazine sensors.

Owing to the superior sensing parameters, spindle-like Co_3O_4- ZnO nanocomposites is a quite promising pathway for developing non-enzymatic hydrazine sensors.

© Engineered Science Publisher LLC 2021

Table 3. Comparison of amperometric responses of modified electrodes for electrocatalytic detection of hydrazine.

Electrode Material	Sensitivity ($\mu A\ \mu M^{-1}cm^{-2}$)	LDR (μM)	LOD (μM)	Ref.
PEDOT:PSS/ZnO	0.14	10–500	5.0	[77]
ZnO nanorods/Au	0.0038	3.0–300	2.0	[78]
Ag-doped ZnO nanoellipsoids	9.46	0.07-1.0	0.07	[79]
Nano-Au ZnO-MWCNT	0.0428	0.5–1800	0.15	[80]
ZnO nanoparticles/Au	1.6	0.066–425	0.066	[81]
Polythiophene (PTh)/mesoporous ZnO	1.22	0.5 – 48	0.207	[82]
Sn/ZnO NPs	5.0108	0.002–200	18.95	[83]
Mesoporous Au/ZnO	0.873	0.2–14.2	0.242	[84]
ZrO_2 NPs/Au electrode	8.99	-	1.05	[85]
Spindel shaped Co_3O_4 -ZnO nanocomposites /Au	23.15	0.05-2.35	0.05	This work

3.4 Proposed mechanism for sensing behavior of spindle-like Co_3O_4-ZnO nanocomposites

The formation of p-n heterojunctions in Spindle-like Co_3O_4-ZnO nanocomposites lowers the conductance and enhances the resistance of the nanomaterials in the air (O_2).[54,86] This is attributed to the consumption of the CB electrons for the formation of oxygenated anionic and free radical species like $O_2^{-\bullet}$, $HO_2^{\bullet}$, O_2^-, O_2^{2-}, $O^{2-}$and $HO^{\bullet}$ from the adsorbed O_2 on the surface of the nanomaterials as mentioned earlier in the photocatalytic mechanism.[87,88] Though, the density of these species is much more under UV light irradiation which is favorable for the fast degradation of the dyes. Additionally, the electron-depletion layer and hole-accumulation layers are also formed near the surfaces of the Co_3O_4 and ZnO components, respectively.[89–91] The surface adsorbed oxygenated species oxidize the hydrazine as soon as it comes in contact with the nanoparticles. The $H^{\bullet}$ radical abstraction has also been reported from the N_2H_4 molecules by the $OH^{\bullet}$ radicals.[92] This oxidation discharges the electrons which are moved back to the CB of the Co_3O_4 and ZnO leading to decreased resistance and increased conductivity. Thus, an increase in the concentration of the N_2H_4 increases the current potentials of the nanomaterials as is observed in this study.

$$N_2H_4+O_2^- \rightarrow N_2+2H_2O+e^- \quad (11)$$

$$N_2H_4+2O^{2-} \rightarrow N_2+2H_2O+4e^- \quad (12)$$

$$N_2H_4+O_2^{2-} \rightarrow N_2+2H_2O+2e^- \quad (13)$$

$$N_2H_4+OH^{\bullet} \rightarrow N_2H_3^{\bullet}+2H_2O \quad (14)$$

The proposed sensing mechanism for the electrochemical sensing of N_2H_4 is shown in Fig. 9.

4. Conclusion

In conclusion, we have successfully grown spindle-like Co_3O_4-ZnO nanocomposites via the facile solution process. Various characterization techniques viz (XRD, FESEM, EDS, FTIR, and UV) confirm the successful incorporation of cubic Co_3O_4 in the hexagonal ZnO matrix. Spindle-like Co_3O_4- ZnO nanocomposites showed excellent photocatalytic as well as electrochemical sensing properties. We observed that the incorporation of Co_3O_4 to the enhancement of surface area and hence increase in photocatalytic as well as chemical sensing efficiency. Hence it can be concluded that optimal Co_3O_4 doping in ZnO results in a remarkable increase in photocatalytic as well as sensing applications owing to separation of charge carriers resulting in restricting their recombination. Therefore, spindle-like Co_3O_4-ZnO nanomaterials are a promising candidate for photocatalytic degradation of hazardous substances as well as for electrochemical sensing applications.

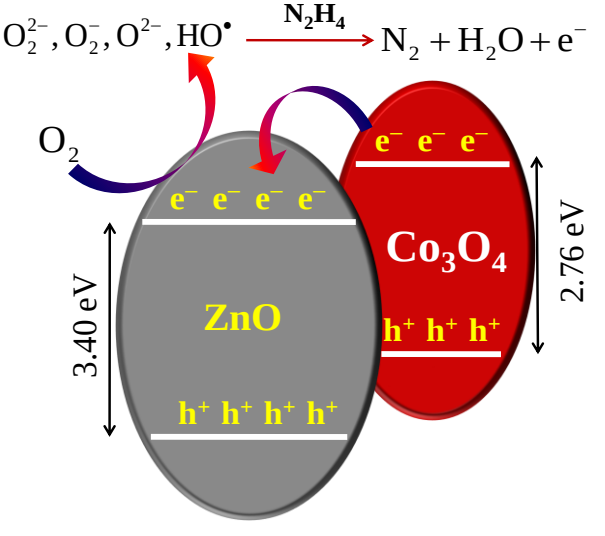

Fig. 9 Proposed mechanism of electrochemical sensing of hydrazine by spindle-like Co_3O_4- ZnO nanocomposites modified Au electrode.

Acknowledgment

R. Kumar acknowledges the CSIR, New Delhi for the award of SRF. Ahmad Umar would like to acknowledge the support of Najran University, Kingdom of Saudi Arabia.

Conflict of interest

There are no conflicts to declare.

Supporting information

Not applicable.

References

[1] H. Zhao, W. Deng and Y. Li, *Adv. Compos. Hybrid Mater.*, 2018, **1**, 404–413, doi: 10.1007/s42114-017-0015-0.

[2] S. Kaplan, *Crit. Rev. Environ. Sci. Technol.*, 2013, **43**, 1074–

© Engineered Science Publisher LLC 2021

1116, doi: 10.1080/10934529.2011.627036.
[3] N. Asif and M. Malik, *Pollution*, 2018, **4**, 111–118, doi: 10.22059/poll.2017.237440.296.
[4] Yu Meiyan, T. Yu, S. Chen, Z. Guo and I. Seok, *ES Mater. Manuf.*, 2020, **7**, 64–69, doi: 10.30919/esmm5f712.
[5] J. Núñez, M. Yeber, N. Cisternas, R. Thibaut, P. Medina and C. Carrasco, *J. Hazard. Mater.*, 2019, **371**, 705–711, doi: 10.1016/j.jhazmat.2019.03.030.
[6] A. Ali, I.A. Shaikh, T. Abid, F. Samina, S. Islam, A. Khalid, N. Firdous and M.T. Javed, *Polish J. Environ. Stud.*, 2019, **28**, 2565–2570, doi: 10.15244/pjoes/91940.
[7] F. Sabouhi, M.S. Pishvaee and M.S. Jabalameli, *Comput. Ind. Eng.*, 2018, **126**, 657–672, doi: 10.1016/j.cie.2018.10.001.
[8] Y.-J. Jing, Ya-Jie; Kang, Le; Du, Hui-Ling; Du, Xian; Jing, Xin-Rui; Bai, Long ; Zhang, *Sci. Adv. Mater.*, 2020, **12**, 1695–1701, doi: 10.1166/sam.2020.3911.
[9] M. Chen, J. Zhu, B. Yang, X. Yao, X. Zhu, Q. Liu and X. Lyu, *Adv. Compos. Hybrid Mater.*, 2018, **1**, 612–623, doi: 10.1007/s42114-018-0045-2.
[10] Y. Chen, Xue; Pei, *Sci. Adv. Mater.*, 2020, **12**, 435–440, doi: 10.1166/sam.2020.3607.
[11] M.J. Babu, S.M. Botsa, S.J. Rani, B. Venkateswararao and R. Muralikrishna, *Adv. Compos. Hybrid Mater.*, 2020, **3**, 205–212, doi: 10.1007/s42114-020-00149-1.
[12] N.T. Nandhini, S. Rajeshkumar and S. Mythili, *Biocatal. Agric. Biotechnol.*, 2019, **19**, 101138, doi: 10.1016/j.bcab.2019.101138.
[13] A. Tkaczyk, K. Mitrowska and A. Posyniak, *Sci. Total Environ.*, 2020, **717**, 137222, doi: 10.1016/j.scitotenv.2020.137222.
[14] S. Miao, Yingchun; Xu, Xiaolin; Liu, Kaiquan; Yu, Shiwen; Wang, Yaqin; Yang, *Sci. Adv. Mater.*, 2020, **12**, 1027–1033, doi: 10.1166/sam.2020.3752.
[15] Guo Siyao, J. Shang, T. Zhao, D. Hou, Z. Jin and G. Sun, *ES Mater. Manuf.*, 2018, **2**, 24–27, doi: 10.30919/esmm5f168.
[16] F. Lu and D. Astruc, *Coord. Chem. Rev.*, 2020, **408**, 213180, doi: 10.1016/j.ccr.2020.213180.
[17] R. Gusain, K. Gupta, P. Joshi and O.P. Khatri, *Adv. Colloid Interface Sci.*, 2019, **272**, 102009, doi: 10.1016/j.cis.2019.102009.
[18] H. Yuan, H. Peng, J. Guan, Y. Liu, J. Dai, R. Su, Z. Guo, Y. Chen, Q. Hu, B. Yuan *et al.*, *Eng. Sci.*, 2020, **9**, 68–76, doi: 10.30919/es8d910.
[19] J. Ma, Xiangrong; Dang, Rui; Liu, Jieying; Yang, Fang; Li, Huigui; Zhang, Yuxin; Luo, *Sci. Adv. Mater.*, 2020, **12**, 357–365, doi: 10.1166/sam.2020.3549.
[20] R. Kumar, G. Kumar and A. Umar, *Nanosci. Nanotechnol. Lett.*, 2014, **6**, 631–650, doi: 10.1166/nnl.2014.1879.
[21] M. Danish, M. Qamar, M.H. Suliman and M. Muneer, *Adv. Compos. Hybrid Mater.*, 2020, **3**, 570–582, doi: 10.1007/s42114-020-00187-9.
[22] X. Liu, Ruiping; Mao, Jia; Li, *J. Nanoelectron. Optoelectron.*, 2020, **15**, 250–256, doi: 10.1166/jno.2020.2697.
[23] Zhao Zengying, H. Ma, M. Feng, Z. Li, D. Cao and Z. Guo, *Eng. Sci.*, 2019, **7**, 52–58, doi: 10.30919/es8d689.
[24] R. Kumar, G. Kumar, M.S. Akhtar and A. Umar, *J. Alloys Compd.*, 2015, **629**, 167–172, doi: 10.1016/j.jallcom.2014.12.232.
[25] A. Umar, R. Kumar, G. Kumar, H. Algarni and S.H. Kim, *J. Alloys Compd.*, 2015, **648**, 46–52, doi: 10.1016/j.jallcom.2015.04.236.
[26] R. Kumar, G. Kumar and A. Umar, *Mater. Lett.*, 2013, **97**, 100–103, doi: 10.1016/j.matlet.2013.01.044.
[27] A.B.A. Baig, V. Rathinam and V. Ramya, *Adv. Compos. Hybrid Mater.*, 2021, **4**, 114–126, doi: 10.1007/s42114-017-0015-0.
[28] A.A. Ibrahim, A. Umar, R. Kumar, S.H. Kim, A. Bumajdad and S. Baskoutas, *Ceram. Int.*, 2016, **42**, 16505–16511, doi: 10.1016/j.ceramint.2016.07.061.
[29] Z.A. Mishra, Sapna; Chishti, Benazir; Fouad, H.; Seo, H. K.; Ansari, *Sci. Adv. Mater.*, 2020, **12**, 220–227, doi: 10.1166/sam.2020.3700.
[30] A. Yadav, Y. Upadhyay, R.K. Bera and S.K. Sahoo, *Food Chem.*, 2020, **320**, 126611, doi: 10.1016/j.foodchem.2020.126611.
[31] D.Y. Nadargi, R.B. Dateer, M.S. Tamboli, I.S. Mulla and S.S. Suryavanshi, *RSC Adv.*, 2019, **9**, 33602–33606, doi: 10.1039/c9ra06482f.
[32] Y. Al-Hadeethi, A. Umar, A.A. Ibrahim, S.H. Al-Heniti, R. Kumar, S. Baskoutas and B.M. Raffah, *Ceram. Int.*, 2017, **43**, 6765–6770, doi: 10.1016/j.ceramint.2017.02.088.
[33] S. Bagyalakshmi, A. Sivakami and K.S. Balamurugan, *Obes. Med.*, 2020, **18**, 100229, doi: 10.1016/j.obmed.2020.100229.
[34] L. Cheng, Hao; Zhou, Zhengyuan; Qin, Danfeng; Huang, Wenyi; Feng, Jun; Tang, Tingfan; Hu, Guangzhi; Li, *Sci. Adv. Mater.*, 2020, **12**, 693–700, doi: 10.1166/sam.2020.3709.
[35] R. Kumar, A. Umar, G. Kumar, H.S. Nalwa, A. Kumar and M.S. Akhtar, *J. Mater. Sci.*, 2017, **52**, 4743–4795, doi: 10.1007/s10853-016-0668-z.
[36] Q. Shi, K. Ling, S. Duan, X. Wang, S. Xu, D. Zhang, Q. Wang, S. Li, L. Zhao and W. Wang, *Spectrochim. Acta - Part A Mol. Biomol. Spectrosc.*, 2020, **231**, 118096, doi: 10.1016/j.saa.2020.118096.
[37] Jadhav Pranav, S. Shinde, S.S. Suryawanshi, Shivan, B. Teli, P.S. Patil, A. A. Ramteke, H.N. G. and N.R. Prasad, *Eng. Sci.*, 2020, **12**, 79–94, doi: 10.30919/es8d1138.
[38] R. Kumar, A. Umar, G. Kumar and H.S. Nalwa, *Ceram. Int.*, 2017, **43**, 3940–3961, doi: 10.1016/j.ceramint.2016.12.062.
[39] Bag Partha Pratim, G.P. Singh, S. Singha and G. Roymahapatra, *Eng. Sci.*, 2020, **13**, 1–10, doi: 10.30919/es8d1166.
[40] L. Zhang, Q. Liang, P. Yang, Y. Huang, W. Chen, X. Deng, H. Yang, J. Yan and Y. Liu, *Int. J. Hydrogen Energy*, 2019, **44**, 24209–24217, doi: 10.1016/j.ijhydene.2019.07.146.
[41] Y. Li, F.M. Li, X.Y. Meng, S.N. Li, J.H. Zeng and Y. Chen, *ACS Catal.*, 2018, **8**, 1913–1920, doi: 10.1021/acscatal.7b03949.
[42] L. Li, Q. Xu, Y. Zhang, J. Li, J. Fang, Y. Dai, X. Cheng, Y. You and X. Li, *J. Alloys Compd.*, 2020, **823**, 153750, doi: 10.1016/j.jallcom.2020.153750.
[43] Y. Lu, W. Yang, W. Li, M. Chen, L. Shuai, P. Qi, D. Zhang, H. Du, Y. Tang and M. Qiu, *J. Alloys Compd.*, 2020, **818**, 152877,

© Engineered Science Publisher LLC 2021

doi: 10.1016/j.jallcom.2019.152877.
[44] Y. Wang, R. Guo, W. Liu, L. Zhu, W. Huang, W. Wang and H. Zheng, *J. Power Sources*, 2019, **444**, 227260, doi: 10.1016/j.jpowsour.2019.227260.
[45] J.M. Xu and J.P. Cheng, *J. Alloys Compd.*, 2016, **686**, 753–768, doi: 10.1016/j.jallcom.2016.06.086.
[46] D. Bekermann, A. Gasparotto, D. Barreca, C. Maccato, E. Comini, C. Sada, G. Sberveglieri, A. Devi and R.A. Fischer, *ACS Appl. Mater. Interfaces*, 2012, **4**, 928–934, doi: 10.1021/am201591w.
[47] D. Zhu, F. Zheng, S. Xu, Y. Zhang and Q. Chen, *Dalt. Trans.*, 2015, **44**, 16946–16952, doi: 10.1039/c5dt02271a.
[48] Y. Liu, X. Zhang, B. Wu, H. Zhao, W. Zhang, C. Shan, J. Yang and Q. Liu, *Chem. Sel.*, 2019, **4**, 12445–12454, doi: 10.1002/slct.201903620.
[49] Y. Yang, X. Wang, G. Yi, H. Li, C. Shi, G. Sun and Z. Zhang, *Nanomaterials*, 2019, **9**, 1599, doi: 10.3390/nano9111599.
[50] G. Mohamed Reda, H. Fan and H. Tian, *Adv. Powder Technol.*, 2017, **28**, 953–963, doi: 10.1016/j.apt.2016.12.025.
[51] M. Hassanpour, H. Safardoust-Hojaghan and M. Salavati-Niasari, *J. Mol. Liq.*, 2017, **229**, 293–299, doi: 10.1016/j.molliq.2016.12.090.
[52] Y. Yang, W. Cheng and Y.F. Cheng, *Appl. Surf. Sci.*, 2019, **476**, 815–821, doi: 10.1016/j.apsusc.2019.01.157.
[53] S. Park, S. Kim, H. Kheel and C. Lee, *Sens. Actuators B Chem.*, 2016, **222**, 1193–1200, doi: 10.1016/j.snb.2015.08.006.
[54] Y. Li, K. Li, Y. Luo, B. Liu, H. Wang, L. Gao and G. Duan, *Sens. Actuators B Chem.*, 2020, **308**, 127657, doi: 10.1016/j.snb.2020.127657.
[55] S. Wang, J. Cao, W. Cui, L. Fan, X. Li, D. Li and T. Zhang, *Sens. Actuators B Chem.*, 2019, **297**, 126746, doi: 10.1016/j.snb.2019.126746.
[56] P. Yan, M. Huang, B. Wang, Z. Wan, M. Qian, H. Yan, T.T. Isimjan, J. Tian and X. Yang, *J. Energy Chem.*, 2020, **47**, 299–306, doi: 10.1016/j.jechem.2020.02.006.
[57] Y. Al-Hadeethi, A. Umar, S.H. Al-Heniti, R. Kumar, S.H. Kim, X. Zhang and B.M. Raffah, *Ceram. Int.*, 2017, **43**, 2418–2423, doi: 10.1016/j.ceramint.2016.11.031.
[58] R. Kumar, A. Umar, G. Kumar, M.S. Akhtar, Y. Wang and S.H. Kim, *Ceram. Int.*, 2015, **41**, 7773–7782, doi: 10.1016/j.ceramint.2015.02.110.
[59] G. Kumar, R. Kumar, S.W. Hwang and A. Umar, *J. Nanosci. Nanotechnol.*, 2014, **14**, 7161–7166, doi: 10.1166/jnn.2014.9229.
[60] A.L. Patterson, *Phys. Rev.*, 1939, **56**, 978–982, doi: 10.1103/PhysRev.56.978.
[61] A.H. Jawad, N.S.A. Mubarak, M.A.M. Ishak, K. Ismail and W.I. Nawawi, *J. Taibah Univ. Sci.*, 2016, **10**, 352–362, doi: 10.1016/j.jtusci.2015.03.007.
[62] C.M. Magdalane, K. Kaviyarasu, J.J. Vijaya, B. Siddhardha, B. Jeyaraj, J. Kennedy and M. Maaza, *J. Alloys Compd.*, 2017, **727**, 1324–1337, doi: 10.1016/j.jallcom.2017.08.209.
[63] J. Tian, Q. Shao, J. Zhao, D. Pan, M. Dong, C. Jia, T. Ding, T. Wu and Z. Guo, *J. Colloid Interface Sci.*, 2019, **541**, 18–29, doi: 10.1016/j.jcis.2019.01.069.
[64] C. Lops, A. Ancona, K. Di Cesare, B. Dumontel, N. Garino, G. Canavese, S. Hérnandez and V. Cauda, *Appl. Catal. B Environ.*, 2019, **243**, 629–640, doi: 10.1016/j.apcatb.2018.10.078.
[65] Y. Liu, H. Guo, Y. Zhang, X. Cheng, P. Zhou, G. Zhang, J. Wang, P. Tang, T. Ke and W. Li, *Sep. Purif. Technol.*, 2018, **192**, 88–98, doi: 10.1016/j.seppur.2017.09.045.
[66] M. Sundararajan, V. Sailaja, L. John Kennedy and J. Judith Vijaya, *Ceram. Int.*, 2017, **43**, 540–548, doi: 10.1016/j.ceramint.2016.09.191.
[67] K.A. Adegoke, M. Iqbal, H. Louis and O.S. Bello, *Mater. Sci. Energy Technol.*, 2019, **2**, 329–336, doi: 10.1016/j.mset.2019.02.008.
[68] M.A. Alvi, A.A. Al-Ghamdi and M. ShaheerAkhtar, *Mater. Lett.*, 2017, **204**, 12–15, doi: 10.1016/j.matlet.2017.06.005.
[69] Q.I. Rahman, M. Ahmad, S.K. Misra and M. Lohani, *Mater. Lett.*, 2013, **91**, 170–174, doi: 10.1016/j.matlet.2012.09.044.
[70] K. Rokesh, S.C. Mohan, S. Karuppuchamy and K. Jothivenkatachalam, *J. Environ. Chem. Eng.*, 2018, **6**, 3610–3620, doi: 10.1016/j.jece.2017.01.023.
[71] B. Wang, Bo; Zhang, Ruiling; Xu, Jin; Qin, Songyan; Zheng, Jiajun; Bian, Yewang; Liu, Yang; Shen, *Sci. Adv. Mater.*, 2020, **12**, 449–453, doi: 10.1166/sam.2020.3619.
[72] H. Zheng, Haibin; Bu, *J. Nanoelectron. Optoelectron.*, 2020, **15**, 184–188, doi: 10.1166/jno.2020.2683.
[73] Shinde Dnyaneshwar R., I.S. Quraishi and R.A. Pawar, *ES Energy Environ.*, 2021, **14**, 54-62, doi: 10.30919/esee8c504.
[74] Vairale Priti, V. Sharma, B. Bade, A. Waghmare, P. Shinde, A. Punde, V. Doiphode, R. Aher, S. P, harkar harkar, *Eng. Sci.*, 2020, **11**, 76–84, doi: 10.30919/es8d0023.
[75] Shi Cai, W. Yuan, K. Qu, J. Shi, M. Eqi, X. Tan, Z. Huang, F.Gándara, D. Pan, N. Naik, Y. Zhang, and Z. Guo, *Eng. Sci.*, 2021, **16**, (Accepted Article), doi: 10.30919/es8d478.
[76] H. Wang, L. Zhang, Z. Chen, J. Hu, S. Li, Z. Wang, J. Liu and X. Wang, *Chem. Soc. Rev.*, 2014, **43**, 5234–5244, doi: 10.1039/c4cs00126e.
[77] T. Beduk, E. Bihar, S.G. Surya, A.N. Castillo, S. Inal and K.N. Salama, *Sens. Actuators B Chem.*, 2020, **306**, 127539, doi: 10.1016/j.snb.2019.127539.
[78] A. Umar, M.M. Rahman and Y.B. Hahn, *J. Nanosci. Nanotechnol.*, 2009, **9**, 4686–4691, doi: 10.1166/jnn.2009.1103.
[79] R. Kumar, D. Rana, A. Umar, P. Sharma, S. Chauhan and M.S. Chauhan, *Talanta*, 2015, **137**, 204–213, doi: 10.1016/j.talanta.2015.01.039.
[80] C. Zhang, G. Wang, Y. Ji, M. Liu, Y. Feng, Z. Zhang and B. Fang, *Sens. Actuators B Chem.*, 2010, **150**, 247–253, doi: 10.1016/j.snb.2010.07.007.
[81] W. Sultana, S. Ghosh and B. Eraiah, *Electroanalysis*, 2012, **24**, 1869–1877, doi: 10.1002/elan.201200210.
[82] M. Faisal, F.A. Harraz, A.E. Al-Salami, S.A. Al-Sayari, A. Al-Hajry and M.S. Al-Assiri, *Mater. Chem. Phys.*, 2018, **214**, 126–134, doi: 10.1016/j.matchemphys.2018.04.085.
[83] M.M. Rahman, H.B. Balkhoyor and A.M. Asiri, *RSC Adv.*, 2016, **6**, 29342–29352, doi: 10.1039/c6ra02352e.
[84] A.A. Ismail, F.A. Harraz, M. Faisal, A.M. El-Toni, A. Al-Hajry and M.S. Al-Assiri, *Mater. Des.*, 2016, **109**, 530–538, doi: 10.1016/j.matdes.2016.07.107.

 © Engineered Science Publisher LLC 2021

[85] P. Bansal, G. Bhanjana, N. Prabhakar, J.S. Dhau and G.R. Chaudhary, *J. Mol. Liq.*, 2017, **248**, 651–657, doi: 10.1016/j.molliq.2017.10.098.
[86] Z. Fang, Xuan; Fang, Dan; Zhao, Hongbin; Yuen, Mukfung; Li, Bobo; Fang, Xuan; Fang, Dan; Zhao, Hongbin ; Yuen, Mukfung; Li, Bobo; Quan, Xiaoyu; Xu, Zhikun; Guo, Zhen, Xiaoyu; Xu, Zhikun; Guo, *J. Nanoelectron. Optoelectron.*, 2020, **15**, 1053–1058, doi: 10.1166/jno.2020.2831.
[87] G. Wang, NuerbiYayalikun, X. Mamat, Y. Li, X. Hu, P. Wang, X. Xin and G. Hu, *Sci. Adv. Mater.*, 2020, **12**, 376–382, doi: doi:10.1166/sam.2020.3567.
[88] A. Umar, R. Kumar, H. Algadi, J. Ahmed, M. Jalalah, A.A. Ibrahim, F.A. Harraz, M.A. Alsaiari and H. Albargi, *Adv. Compos. Hybrid Mater.*, 2021, doi: 10.1007/s42114-021-00283-4.
[89] J. Deng, R. Zhang, L. Wang, Z. Lou and T. Zhang, *Sens. Actuators B Chem.*, 2015, **209**, 449–455, doi: 10.1016/j.snb.2014.11.141.
[90] K. Hyo-Joong and L. Jong-Heun, *Sens Actuators B Chem*, 2014, **192**, 607–627, doi: 10.1016/j.snb.2013.11.005.
[91] L. Wang, Z. Lou, R. Wang, T. Fei and T. Zhang, *Sens. Actuators B Chem.*, 2012, **171–172**, 1180–1185, doi: 10.1016/j.snb.2012.06.063.
[92] T.V.T. Mai, H.T. Nguyen and L.K. Huynh, *Phys. Chem. Chem. Phys.*, 2019, **21**, 23733–23741, doi: 10.1039/c9cp04585f.

Author Information

Ramesh Kumar *is serving as Assistant Professor in the Department of Chemistry, Government College Rajgarh, District Sirmaur, Himachal Pradesh. He has completed his Ph.D. at Himachal Pradesh University, Shimla in 2015 in the area of Synthesis Characterization and Applications ZnO Nanostructures. He has been recipient of JRF, SRF from CSIR, New Delhi. He served in Department of Technical Education, Govt. of Himachal Pradesh at Govt. Polytechnic Sundernagar, Mandi H.P. form 2016 to 2018 and trained Diploma students of various trades namely, Civil Engineering, Mechanical Engineering, Computer Science, Architecture Assistantships. He has published 17 research papers in International journals of high Impact factor. Besides he has also presented his research work in 18 National/ International Conferences. Also he has attended 28 National/International Webinars on various current active research fields. As an evident of his active research, he receives the h-index of 12 and i10-index of 13 with total citations of 490 (According to Google scholar).*

Prof. Ahmad Umar *received his Ph.D. in semiconductor and chemical engineering from Chonbuk National University, South Korea. He worked as a research scientist in Brain Korea 21, Centre for Future Energy Materials and Devices, Chonbuk National University, South Korea, in 2007–2008. Afterwards, he joined the Department of Chemistry in Najran University, Najran, Saudi Arabia. He is a distinguished professor of chemistry and served as deputy director of the Promising Centre for Sensors and Electronic Devices (PCSED), Najran University, Najran, Saudi Arabia. Professor Ahmad Umar is specialized in 'semiconductor nanotechnology', which includes growth, properties and their various high technological applications, for instance, gas, chemicals and biosensors, optoelectronic and electronic devices, field effect transistors (FETs), nanostructure-based energy-harvesting devices, such as solar cells, Li-ion batteries, super-capacitors, semiconductor nanomaterial- based environmental remediation, and so on. He is also specialized in the modern analytical and spectroscopic techniques used for the characterizations and applications of semiconductor nanomaterials. He contributed to the world of science by editing world's first handbook series on Metal Oxide Nanostructures and Their Applications (5-volume set, 3500 printed pages, www.aspbs.com/mona) and handbook series on Encyclopedia of Semiconductor Nanotechnology (7-volume set; www.aspbs.com/esn), both published by American Scientific Publishers (www.aspbs.com). He has published more than 600 research papers in reputed journal with h-index of 77 and i10-index of 381 with total citations of over 21000 (According to Google scholar).*

Rajesh Kumar *is presently working as Assistant Professor of Inorganic Chemistry at JC DAV College, Dasuya, Punjab, India. He obtained his B.Sc. Degree in 2001 from Himachal Pradesh University, Shimla and Master degree in 2003 from Guru Nanak Dev University, Punjab. He completed his Ph.D. in 2019 in synthesis, characterization and applications of cellulose based grafted polymers from Punjab Technical University, Jalandhar (Punjab), India. He has authored more than 70 research articles in peer-reviewed international journals. He has authored five book chapters, including three*

© Engineered Science Publisher LLC 2021

chapters in Encyclopedia of Semiconductor Nanotechnology (7-volume set; www.aspbs.com/esn) published by American Scientific Publishers. His present areas of research include synthesis, characterization and applications of nanomaterials and cellulose based grafted polymers.

M. S. Chauhan *is an eminent Professor of Chemistry in the department of Chemistry, Himachal Pradesh University, Shimla, India. His diverse research interest includes solution chemistry of electrolytes, surfactants, and physical chemistry of protein – surfactant interactions in binary solvent systems of aqueous and non-aqueous and mixed non-aqueous solvents. Presently, however, his research focus is on nanoscale materials (composites and doped) and their applications in environmental remediation using various chemicals and dyes as model pollutants in aqueous solutions.*

Girish Kumar *is an Assistant Professor of Physical Chemistry at JCDAV College, Dasuya, Punjab, India since 2004. He obtained B.Sc. (1993) and Ph.D. degrees (2001) from the Himachal Pradesh University, Shimla, and M.Sc. degree (1995) from Kurukshetra University. He was awarded Research Associateship in a CSIR sponsored research project from 2001–2004 at Himachal Pradesh University, Shimla. He has number of research articles in peer-reviewed journals and chapters in edited books to his credit. His present areas of research include solution chemistry of surfactants, surfactant protein interactions & synthesis, characterization, applications of nanomaterials.*

Suvarcha Chauhan *is serving as Professor in the department of chemistry, Himachal Pradesh University, Shimla. She has a remarkable academic and research career. As an alumni of Himachal Pradesh University, Shimla, she has been recipient of several merit scholarships including JRF, SRF and post-doctoral fellowship from CSIR, UGC and Ministry of Environment and Forest. She is not only an excellent core chemistry teacher but also a dedicated researcher since 2001. She has contributed in the world of science by publishing number of research/review articles in the journals of international repute. She has research collaborations with several universities in Kingdom of Saudi Arabia, India, Brazil, Korea, etc. She has served as reviewer for many international journals. As an evident of her active research, she receives the h-index of 35 and i10-index of 117 with total citations of 4614 (According to Google scholar). She remains as a role model as a committed academician and a dedicated researcher.*

Publisher's Note: Engineered Science Publisher remains neutral with regard to jurisdictional claims in published maps and institutional affiliations.

 © Engineered Science Publisher LLC 2021